Journal of Raman Spectroscopy

WILEY

Journal of RAMAN SPECTROSCOPY

RESEARCH ARTICLE

Functionalization of Filter Media for Improved Crystalline Silica Analysis Using Raman Spectroscopy

Mohammadreza Elahifard | Xiaoliang Wang | Judith C. Chow | John G. Watson

Division of Atmospheric Sciences, Desert Research Institute, Reno, Nevada, USA

Correspondence: Xiaoliang Wang (xiaoliang.wang@dri.edu)

Received: 18 May 2024 | **Revised:** 26 July 2024 | **Accepted:** 28 July 2024

Funding: This study was primarily supported by the Desert Research Institute Innovation Research Program (IRP) funds supplemented by NIOSH grant 75D30121C11871.

Keywords: coal dust | hydroxyapatite/AgBr/TiO_2 | photocatalyst | Raman | respirable crystalline silica

ABSTRACT

Respirable crystalline silica (RCS) poses significant health risks in workplaces, including underground coal mines, metal and nonmetal mining, construction sites, fire suppression, and oil and gas industries. Raman spectroscopy offers a promising avenue for direct analysis of RCS on sample filters with minimal pretreatment. However, the presence of organic compounds (OC) in the samples can generate fluorescence signals that interfere with RCS measurements, potentially saturating the detector even at short integration times, particularly when using portable Raman instruments. This study explores a novel approach to address these challenges by functionalizing filters with a hydroxyapatite/silver bromide/titanium dioxide (HAT) photocatalyst, facilitating the oxidation and removal of OC using the Raman excitation laser. Photocatalytic degradation experiments conducted on polyvinyl chloride (PVC) filters preloaded with HAT and anatase titanium dioxide (TiO_2) particles demonstrated that HAT significantly enhances the degradation of OC, such as oxalic acid, under visible light irradiation compared to TiO_2. Additionally, fluorescence interferences were reduced for coal dust samples analyzed on functionalized silver filters using a portable Raman instrument. The efficacy of HAT in OC photocatalytic degradation on silver filters was further confirmed using a benchtop micro-Raman system. Filter functionalization had minimal impact on filtration efficiencies and pressure drops, indicating the feasibility of this approach for improving RCS analysis while maintaining filter performance.

1 | Introduction

Long-term occupational exposure to airborne respirable crystalline silica (RCS) causes detrimental effects to human health in mining, construction, fire suppression, and oil and gas industries [1, 2]. Regulatory methods for RCS analysis use X-ray diffraction (XRD) or Fourier-transform infrared (FTIR) spectroscopy [3–6]. These methods require shipping filter samples to off-site laboratories, with ashing and redeposition prior to analysis. The data are only available several weeks after collection, resulting in delays in dust control and exposure mitigation. Replacing these time-consuming methods with field-based real-time monitoring or direct-on-filter (DoF) FTIR techniques is a research priority of the National Institute for Occupational Safety and Health (NIOSH) [7]. While real-time RCS measurement technologies are still under development [8–11], notable progress has been made on DoF FTIR [12–18]. The DoF analysis places the particle-laden filter directly in the laser beam of a portable FTIR. It does not require pretreatment and the measurement can be performed at the mining site at the end of shift, thus expediting the results to mine operators. Challenges include (1) high limit of detection (LOD) due to the lower sensitivity of portable spectrometers than their larger benchtop counterparts and (2) interferences from organic compounds (OC) and other minerals [19].

Nondestructive portable Raman spectroscopy is an alternative to FTIR for RCS DoF analysis at the end of shift, with LODs potentially lower than those of FTIR [11, 20, 21]. However, RCS Raman spectroscopy has interferences from organic-rich materials, such as coal mine dust, due to their fluorescence effects [22]. These effects reduce the RCS signal-to-noise ratios and contribute to the background spectrum and may even saturate the detector. Decreasing the signal integration time or reducing the laser power could mitigate fluorescence to some extent, but it would also lower Raman sensitivity. Selecting an infrared laser wavelength such as 1064 nm can also reduce fluorescence [23]. However, this wavelength can induce more heating of coal samples, potentially causing thermal damages even at a low laser power.

Photooxidation is an efficient method to remove OC while keeping minerals intact. This approach holds promise for mitigating OC fluorescence in the DoF Raman spectra. Titanium dioxide (TiO_2) with an anatase crystal structure has been used as a photocatalyst for the oxidation of OC due to its unique photochemical properties [24, 25]. TiO_2 photocatalysis offers several advantages, including low cost, stability, and environmental friendliness. Its main drawbacks are the limited photocatalytic activity under visible light (VL; $\lambda = 400–700$ nm) and lack of adsorption capacity for organics. However, TiO_2 can be combined with photo-sensitive materials to increase the photo-oxidation efficiencies in VL [26]. Among several photo-sensitive materials that could be combined with TiO_2, silver halides (AgX) have higher efficiency for degradation of hazardous materials [27]. AgX are unstable under VL irradiation as the photo-generated electrons will combine with a mobile interstitial silver ions, leading to the separation of silver atom. However, AgX can be stabilized by TiO_2, and the combined AgX/TiO_2 systems show high stability and photocatalytic activity [28]. Under VL irradiation, only the AgX component in AgX/TiO_2 generates electron–hole pairs; however, in ultraviolet (UV; $\lambda = 100–400$ nm) irradiation, both AgX and TiO_2 could generate electron–hole pairs, enhancing the photo-oxidation efficiency [29]. On the other hand, apatite (a group of calcium phosphate minerals), particularly hydroxyapatite (HA), is known for its strong adsorption properties. It has a unique crystal structure with a high specific surface area to adsorb various contaminants, including OCs. HA finds extensive use in environmental treatment systems and as a biomaterial, owing to its biocompatibility and strong adsorption properties. When combined with TiO_2, HA acts as a bio-ceramic, thereby amplifying the absorbability of TiO_2. This augmentation allows TiO_2 to directly oxidize OC, complementing the oxidation process facilitated by photo-generated free radicals.

Decades of research have been dedicated to the exploration of TiO_2-based nanocomposites, with a particular emphasis on HA/silver bromide/titanium dioxide (HAT) nanocomposites [26, 29, 30, 31]. These nanocomposites have demonstrated capabilities in the photooxidation of organics, even under VL irradiation. This study explores the feasibility of filter functionalization with HAT powders prior to sample collection, with the aim of oxidizing OC to reduce fluorescence during Raman analysis. The objectives are as follows: (1) verify the effects of filter functionalization with the photocatalyst on filtration efficiency and pressure drop, (2) evaluate photooxidation activity of the functionalized filters through photodegradation of oxalic acid (OA), and (3) examine the effects of photocatalyst functionalization on coal mine dust using portable and benchtop Raman systems. Results from this study provide an approach for improving Raman analysis of complex environmental samples such as RCS in coal mine dust.

2 | Experimental

2.1 | Materials

The laboratory testing involves depositing OA, graphite, coal, and RCS powders onto plain and functionalized filter substrates prior to Raman analysis. OA and graphite were purchased from Sigma-Aldrich Company. Brown coal dust samples were obtained by pulverizing bulk samples collected from a coal seam in a West Virginia (WV) underground mine. Elemental (C, H, N, S, and O) analysis [32] shows that the coal sample has a carbon content of 74% (Table S1), indicating that it is bituminous coal [33]. Additionally, the XRD spectrum (Figure S1) indicates the presence of a small amount of crystalline minerals in this sample, such as kaolinite, calcite, pyrite, and α-quartz. Cristobalite or tridymite was not observed. The RCS standard used MIN-U-SIL 5 (U.S. Silica), a type of fine ground silica with a nominal mass median diameter of 1.6 μm, SiO_2 purity > 99.9%, and percentage crystallinity of 88.7% [34, 35]. To synthesize HAT powders, TiO_2 (anatase nanopowder < 100 nm), HA (nanopowder < 200 nm), silver nitrate ($AgNO_3$), ammonium hydroxide, and hexadecyltrimethylammonium bromide were purchased from Sigma-Aldrich Company. The anatase TiO_2 was chosen not only for its higher photocatalytic activity [36] but also because the Raman peak of rutile TiO_2 at 445 cm^{-1} can interfere with the characteristic Raman peak of α-quartz (465 cm^{-1}).

Polyvinyl chloride (PVC) filters have been used for sampling silica, metals, and dust in mining and workplace environments due to their low flow resistance, tare weight, good chemical compatibility, low gaseous absorption, and minimal interference with RCS measurement [37]. Therefore, the 37-mm GLA-5000 PVC filters with a nominal pore size of 5 μm were selected for filtration efficiency, pressure drop, and FTIR analyses. However, a previous study comparing PVC and silver membrane filters found that PVC filters have spectral interferences with the α-quartz peak at 465 cm^{-1}, while silver filters enhance Raman scattering from the silver membrane [11]. Therefore, 37-mm diameter SKC silver membrane filters (Part Number: 225-1801) with a nominal pore size of 0.8 μm and thickness of 50 μm were used for Raman analysis.

2.2 | Preparation of HAT Nanoparticles With 5% HA

HAT nanocomposite particles, consisting of 5% HA, were synthesized through a deposition method [30]. An aqueous suspension was created by adding 1.0 g of TiO_2 and 0.1 g of HA to 100 mL of distilled deionized water (DDW), followed by magnetic stirring. Subsequently, 1.2 g of hexadecyl trimethyl ammonium bromide was introduced into the suspension. While maintaining magnetic stirring, a solution containing 0.21 g of $AgNO_3$ dissolved in 2.3 mL of ammonium hydroxide (NH_4OH) with 25 wt% ammonia (NH_3) was swiftly added to the mixture. The resulting suspension required continuous stirring at room

temperature for 18 h to facilitate the formation of HAT nanoparticles with the desired composition [26]. Lastly, the synthesized photocatalyst was subjected to calcination in air at 500°C for 3 h.

2.3 | Filter Functionalization and Characterization

TiO_2 and HAT photocatalysts were deposited on PVC filters (referred to as TiO_2_PVC and HAT_PVC filters for TiO_2 and HAT, respectively) by impregnating filters through a Buchner funnel with a photocatalyst suspension in ethanol. The suspension volume was adjusted to achieve a mass loading of ~0.5–2 mg of photocatalyst per filter. For silver membrane filters, a 1 mg/mL HAT suspension was prepared in DDW, which was placed in an ultrasonic bath for 5 min and agitated for 10 to 20 s using a vortex mixer. A 0.1 mL of the suspension was deposited onto silver membrane filter with spot area of ~1-cm diameter using the drop-casting method. The filters (referred to as HAT silver filters) were dried on a hotplate for 5 min.

The morphology, particle size, crystalline structure, and elemental composition of the prepared HAT samples have been characterized previously [26]. The elemental concentrations of the HAT-functionalized PVC filters were measured by energy dispersive X-ray fluorescence (EDXRF) (Model: Epsilon 5, PANalytical) analysis, showing the presence of all the HAT elements including P, Ca, Ti, Ag, and Br (Table 1).

2.4 | Filtration Efficiency and Pressure Drop Measurement

The filtration efficiency and pressure drop for plain 37-mm PVC and HAT_PVC filters were measured with a setup similar to that reported previously [19, 38]. Polydisperse sodium chloride (NaCl) particles were generated by nebulizing a 0.5% aqueous salt solution using a constant output atomizer (Model 3076, TSI Inc.). The dried aerosols were delivered to the test or bypass routes at a flow rate of 2.5 L/min, corresponding to the design flow of the Zefon aluminum cyclone. The particle size distributions before (bypass route) and after (test route) the test filters were measured by a scanning mobility particle sizer (Model 3936L10, TSI Inc.). Each filter was measured four times. The pressure drop across the test filter was measured with a digital manometer.

2.5 | OA Photodegradation

OA has been commonly used for studying the photocatalytic oxidation behavior of TiO_2 [39], and it was chosen as an OC surrogate to evaluate the photooxidation activity of the functionalized filters. Approximately 1 mL of a 1000-ppm OA solution in ethanol was spiked onto plain PVC, TiO_2_PVC, and HAT_PVC filters, followed by air-drying for 2 h. Photocatalytic oxidation of OA was initiated by exposing the filters to VL irradiation from an 85-W lamp (HPUSN 85 W 110 V 5400 K Compact Fluorescent CFL Balanced Daylight Bulb). This lamp, similar to sunlight, emits light from near UV to near infrared (IR) regions, with strongest irradiance in the VL region [29]. The photodegradation of OA, as indicated by its IR absorption, was analyzed using a benchtop FTIR spectrometer (VERTEX 70, Bruker). Prior to each measurement, the FTIR chamber was purged with nitrogen for 3 min to remove water vapor and carbon dioxide interferences. Spectra were recorded in absorbance mode at a spectral resolution of 4 cm^{-1} within a range of 4000–400 cm^{-1}. A blank filter spectrum was recorded to correct for background IR absorption by the filter media.

2.6 | Coal Dust Raman Analysis

For Raman analysis, three types of samples were prepared: 1000-ppm water suspensions of graphite, brown coal, and a 1:1 brown coal + RCS mixture by weight (this high RCS concentration was used due to the low sensitivity of portable Raman for RCS). The suspensions were deposited onto plain silver and HAT silver filters using the drop casting method. For regular and highly concentrated deposition, a volume of 0.05- to 0.2-mL sample suspension was applied, corresponding to 50 μg and 200 μg per filter, respectively. The samples deposited on filters were analyzed using a portable Raman spectrometer (i-Raman, B&W Tek) or a benchtop micro-Raman spectrometer (LabRAM HR Evolution, HORIBA). The excitation wavelength of both instruments is 532 nm with a maximum power of 42 and 500 mW, respectively. Depending on the objective being used, the micro-Raman laser spot size is 0.5–10 μm, while the spot diameter illuminated by the portable Raman laser is about 100 μm. For coal composition analysis, past studies recommended using laser powers lower than 10 mW to prevent coal burning under the laser heating [40]. The Raman spectra were collected using 8.4- and 5-mW laser power at the source, corresponding to 20% and 1% of the maximum power for the portable and benchtop Raman, respectively. These power levels ensured that the coal dust samples were not exposed to excessive energy that could lead to burning. Since the excitation laser wavelength is in the VL region, and pure TiO_2 is not active at 532 nm, only HAT_ filters were evaluated by Raman analysis. Depending on mass loading and the Raman instrument, various integration times (2 s to 5 min) were used. The signal intensities for quartz

TABLE 1 | Mass and elemental concentrations of PVC filters loaded with different amounts of HAT (hydroxyapatite/silver bromide/titanium dioxide).

Filters	Loading mass (mg)	P (μg/filter)	Ca (μg/filter)	Ti (μg/filter)	Ag (μg/filter)	Br (μg/filter)
HAT_PVC_1	0.45	0.0	16.3	53.9	81.9	110.5
HAT_PVC_2	1.66	9.2	58.5	203.2	408.3	550.0
HAT_PVC_3	2.19	13.2	70.8	252.9	558.0	760.5

(at 465 cm^{-1}), carbon D-band (disorder, at ~1300 cm^{-1}) and G-band (graphite, at ~1550 cm^{-1}), and anatase TiO_2 (at 147, 396, 512, and 638 cm^{-1}) were calculated as the peak heights at their characterized Raman shifts after baseline correction.

3 | Results

3.1 | Filtration Efficiencies and Pressure Drops

Figure 1 shows that the filtration efficiencies were ≳96% for plain PVC and HAT_PVC filters across an aerodynamic particle diameter range of 18–307 nm. The filtrations' efficiencies were similar for particles ≲25 nm. However, the plain PVC filters showed higher efficiencies than the HAT_PVC filters for particles >25 nm. It is possible that some predeposited HAT particles could be released from the filter, resulting in lower filtration efficiencies. HAT particle impregnation should be optimized in future tests to minimize particle breakthroughs while offering sufficient contact with collected particles for photooxidation.

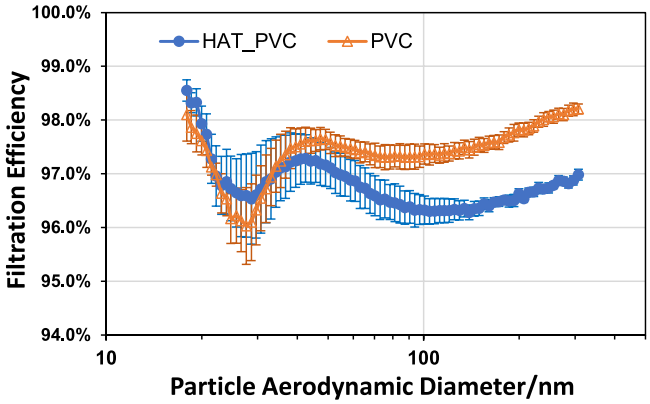

FIGURE 1 | Measured filtration efficiencies for plain PVC and HAT_PVC (with 1-mg HAT) as a function of aerodynamic particle diameter. The error bars represent standard error of four repeated tests for each type of filter at each size. Data above 307 nm were not included due to low counting statistics.

Future experiments should also measure the filtration of particles >300 nm.

As anticipated, the pressure drop across the HAT_PVC filter (0.4 kPa) was slightly higher than that of the plain PVC filter (0.3 kPa). These pressure drops are much lower than the maximum pressure drop (7 kPa) that can be compensated for by the Escort ELF personal sampling pump which is commonly used for mining and workplace dust sampling. These results demonstrate that PVC filters functionalized with HAT particles have similar filtration properties as the plain PVC filters.

3.2 | Photocatalytic Degradation of OA

To evaluate the photocatalytic degradation of OA, three types of PVC filters (i.e., plain PVC, TiO_2_PVC, and HAT_PVC) loaded with approximately 1-mg OA were subjected to VL irradiation followed by FTIR analysis. The analysis focused on the FTIR wavenumber range of 3100–3700 cm^{-1} that corresponds to characteristic absorption by OA. Figure 2A shows that on the plain PVC filter, the characteristic FTIR peaks of OA remained unaffected after 2 h of VL exposure, suggesting that OA had minimal degradation when subjected to VL. In contrast, both the TiO_2_PVC (Figure 2B) and HAT_PVC (Figure 2C) filters exhibited marked OA photodegradation under VL irradiation, as shown by the decreased absorption of the OA peak. While it took 1 h to completely oxidize OA on TiO_2_PVC filters, it only took 20 min on the HAT_PVC filters. This result demonstrates that the synthesized photocatalyst, HAT, exhibited enhanced photocatalytic activity as compared to TiO_2, promoting the degradation of OA under VL irradiation.

The mechanisms for HAT to enhance photooxidation depend on increasing the lifetime of the photo-generated electron–hole pairs that actively participate in various oxidation reactions [31, 41]. The photogenerated holes (h^+) in the valence band and the electrons (e^-) in the conduction band contributed to oxidation reactions involving adsorbed OC. Specifically, h^+ could

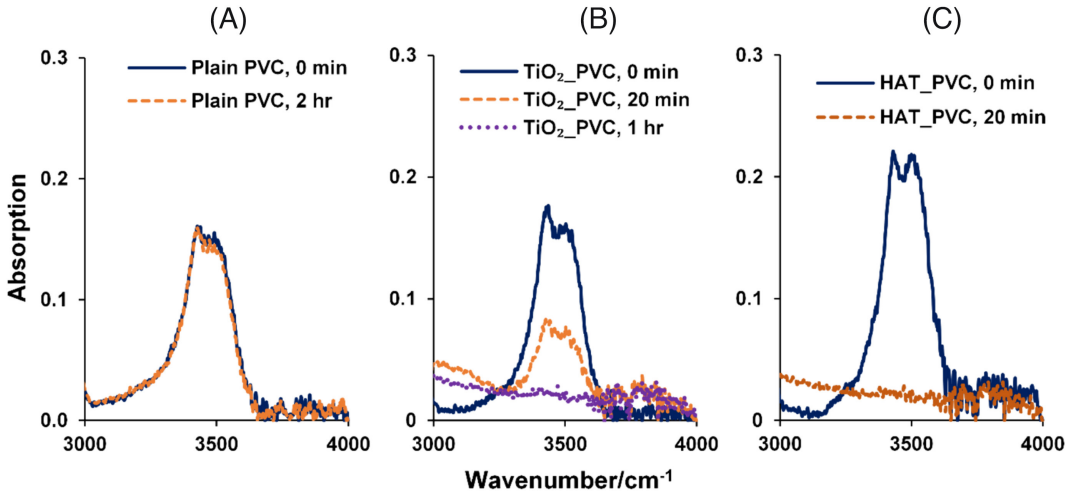

FIGURE 2 | FTIR spectra for three different types of PVC filters: (A) plain PVC; (B) TiO_2_PVC, and (C) HAT_PVC loaded with ~1-mg OA before and after VL irradiation for the durations indicated in the legends. TiO_2_PVC and HAT_PVC filters were loaded with ~1-mg TiO_2 and HAT photocatalyst, respectively.

engage in direct and indirect reactions, either by directly reacting with OC to generate free radicals or oxidizing species, or by indirectly creating hydroxyl radicals (•OH). Meanwhile, e^- are capable of reducing oxygen molecules (O_2) to produce superoxide radicals ($O_2^{\bullet-}$) and •OH, both are potent oxidizing agents [29, 39]. These free radicals or oxidizing species act upon the OC, initiating their degradation into smaller molecules. In certain cases, this process leads to complete oxidation of the OC into CO_2 and H_2O, underscoring the effective photocatalytic potential of HAT in OA degradation.

3.3 | Coal Mine Dust Analysis by a Portable Raman

To evaluate the potential fluorescence interference and detector saturation challenges for organics-rich coal samples, initial experiments tested pure graphite and brown coal samples using the 532-nm portable i-Raman spectrometer with a laser power setting of 8.4 mW for various signal integration times (1–5 min). While the Raman detector was not saturated for pure graphite, it was for brown coal at a signal integration time of 3 min. Carbon analysis shows that the graphite was dominated by elemental carbon, with an organic/elemental carbon ratio of 0.02, while the brown coal had rich organics, with an organic/elemental carbon ratio of 0.3. This observation confirms that the fluorescence was generated primarily by OC content in the coal sample, with elemental carbon having a minimal fluorescence effect.

Figure 3 compares the Raman signals for brown coal and brown coal + RCS samples on plain silver and HAT silver filters. On plain silver filters, Figure 3A shows that neither brown coal nor brown coal + RCS samples show distinct RCS peaks (at 465 cm^{-1}) that are readily discernible from background signals. For the 3-min integration time, the detector saturated at wave numbers > 1200 cm^{-1} while the region around RCS scattering exhibited a wavy background that could interfere with the RCS signal. On the other hand, on HAT silver filters, Figure 3B shows that Raman signals corresponding to TiO_2, quartz, and coal are discernible for the brown coal + RCS sample when the signal integration time was extended to 5 min and the detector was not saturated. These results demonstrate that functionalization of silver filters with a HAT photocatalyst improves the analysis using portable Raman spectrometry. This improvement can be attributed to two factors: (1) HAT efficiently absorbs laser light without inducing fluorescence, analogous to graphite, enabling an extended integration time to increase the RCS signal, and (2) HAT photo-oxidizes OC and quenches the OC fluorescence. Both factors increase RCS signals and lower the minimum detection limits.

3.4 | Coal Mine Dust Analysis by Micro-Raman

Further tests were conducted to evaluate the photooxidation of brown coal dust using the benchtop micro-Raman spectrometer, as it offers higher sensitivity and enables suitable sample analyses with short integration times as compared to portable Raman devices. Figure 4 shows Raman signals for brown coal dust samples on plain silver and HAT silver filters. Data were acquired through five consecutive Raman analysis at the same spatial location, each with a signal integration time of

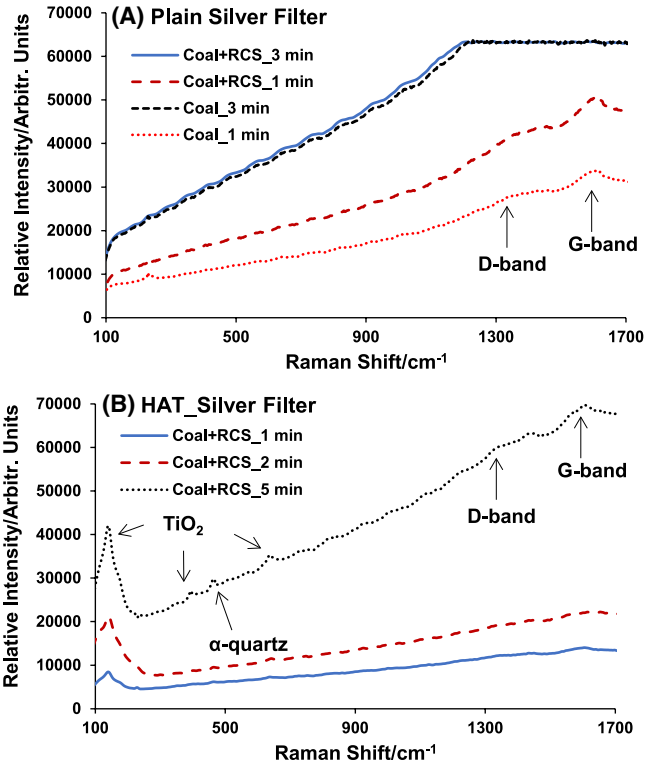

FIGURE 3 | Portable Raman spectra of (A) plain silver membrane filters loaded with coal (50 μg) and coal + RCS (25 μg each) and (B) HAT silver filter loaded with coal + RCS (25 μg each) at different integration times. Raman analysis on each filter was conducted at the same spatial location.

2 s. Similar to the portable Raman result in Figure 3A, Raman spectra on plain silver filters in Figure 4A exhibited a pronounced fluorescence signals from the brown coal particles. When the baseline was subtracted, the coal peaks intensity remained consistent, indicating that the laser power (5 mW) employed was sufficiently low to avoid thermal degradation or destruction of the coal compositions. On the other hand, Raman spectra acquired on HAT silver filters (Figure 4B) did not exhibit high background noise or the fluorescence signals. Furthermore, the intensities of the coal's D and G bands show a distinct downward trend as the analysis progressed on the same spot (Runs 1–5). This trend indicates that the HAT progressively oxidizes OC in the coal sample under the Raman excitation laser irradiation. These findings demonstrate that HAT functionalized silver filters can promote the photocatalytic oxidation of coal to mitigate fluorescence issues during Raman analysis.

To further evaluate the photooxidation of brown coal by HAT, Raman analysis was conducted for a highly concentrated (200 μg/filter) brown coal sample deposited on an HAT silver filter. The analysis was run consecutively with a fixed signal integration time of 10 seconds (Runs 1–4). Figure 5 shows that both D and G bands of coal exhibited significant reduction over the course of the Raman analysis, while the intensities of the TiO_2 peaks increased. The initial spectrum (Run 1) depicted small TiO_2 peaks at specific wavenumbers (396, 512, and 638 cm^{-1}) and prominent coal peaks. After 10 s of laser exposure during the initial Raman analysis, Runs 2–4 show

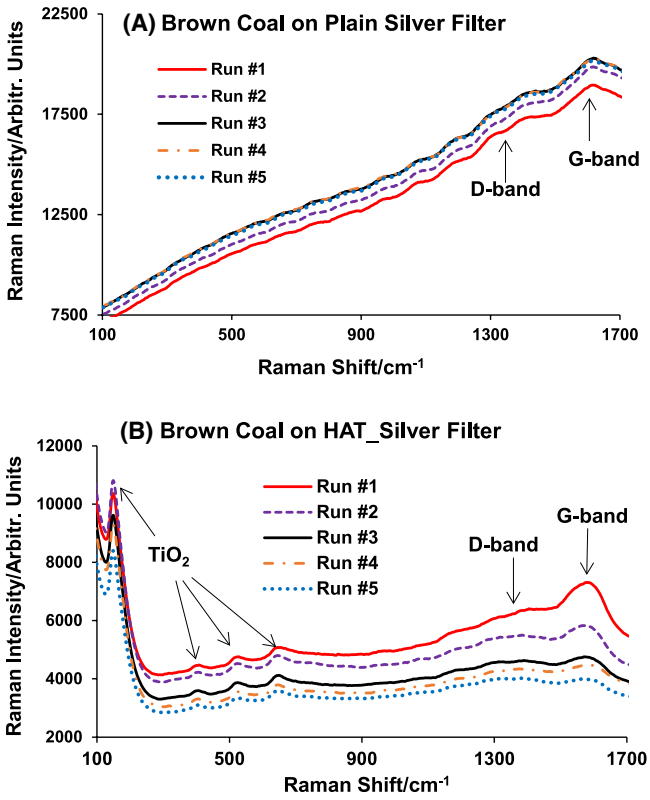

FIGURE 4 | Micro-Raman spectra of 50-μg brown coal dust loaded on (A) plain silver and (B) HAT silver filters at the five consecutive data acquisitions. The integration time for each run was 2 s. The measurement spot was the same on each filter.

much reduced coal D and G bands, accompanied by higher and sharper TiO_2 peaks. This observation indicates that the laser light initially did not fully penetrate the densely loaded dust. The TiO_2 particles were situated beneath the coal dust layer, which reduced the laser light irradiance of TiO_2 particles. As the organic component of the coal dust underwent photooxidation, more TiO_2 particles became accessible to the laser light, resulting in greater TiO_2 peak intensities. These findings demonstrate that HAT can promote the photocatalytic degradation of coal during Raman analysis. They also elucidate the effects coal concentrations on the interaction between laser light, coal dust, and HAT particles, ultimately influencing the observed Raman spectral trends. The deposition thickness should be considered for quantitative Raman analysis.

A similar analysis was conducted on HAT silver filters loaded with a high concentration of brown coal + RCS particles. Figure 6 shows that the intensity of the RCS peak remained consistent throughout the Raman analysis, indicating that the RCS Raman signals were not impeded by the coal particles. On the other hand, the coal bands were reduced with the 20-s laser irradiation, while the TiO_2 peaks exhibited enhancement from 10 to 20 s of light exposure, consistent with the observation in Figure 5.

4 | Discussion

This study demonstrates that the functionalization of filters with a HAT photocatalyst improves RCS analysis for coal mine dust samples using Raman spectrometry. This enhancement can be primarily attributed to two factors: (1) HAT absorbs laser light

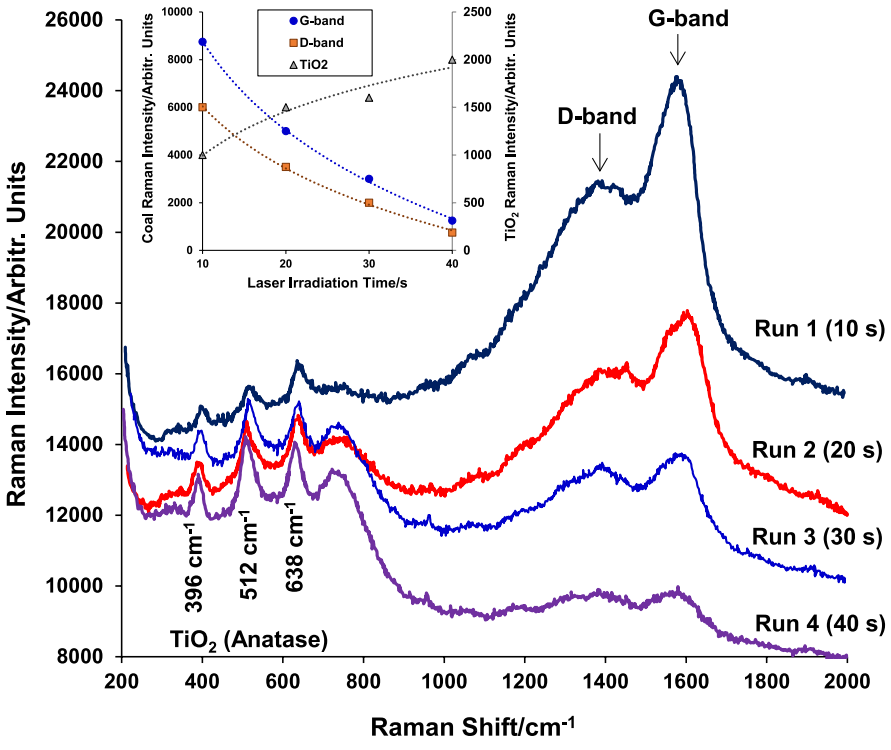

FIGURE 5 | Micro-Raman spectra of 200-μg brown coal dust loaded on HAT silver filter at the four consecutive data acquisitions. The integration time for each run was 10 s. The trends of coal (D-band and G-band) and TiO_2 (at 512 cm^{-1}) Raman intensities are indicated in the inset.

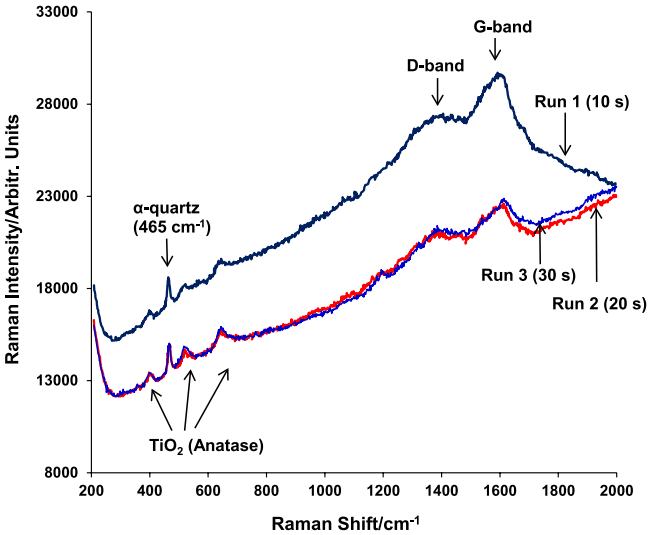

FIGURE 6 | Raman spectra of brown coal + RCS (100 μg each) loaded on HAT silver filter at the three consecutive data acquisitions. The integration time for each run was 10 s.

without inducing fluorescence, thereby allowing for extended signal integration time, and consequently increasing the Raman RCS signal. HAT is positioned beneath the sample, away from the laser direction and Raman detector where this placement ensures that HAT does not intercept the photons emitted from the sample surface, allowing the Raman shift photons to reach the detector without interruption. On the other hand, HAT can absorb some of the fluorescence emitted by the sample, which may be emitted in all directions rather than being reflected towards the detector, thereby may reduce fluorescence signal, and (2) HAT photooxidizes OCs, effectively quenching fluorescence interferences. While this study demonstrates the validity of the second factor, as evidenced by the reduction in coal Raman signals over consecutive analyses, that can be applied for all coal samples experiencing fluorescence issues, further investigation is warranted to fully elucidate the effects of the first factor. Filter functionalization should be examined for nonoxidizable samples, such as mineral mixtures. Such analysis will not only provide deeper insights into the mechanisms underlying the observed enhancements but also pave the way for refining and optimizing the application of HAT-functionalized filters in Raman analyses of diverse sample types.

The portable Raman instrument used in this study did not have sufficient sensitivity for RCS within a 1:1 RCS-coal mixture. Considering that RCS typically constitutes only 5%–20% of coal mine dust, even with filter functionalization, the portable Raman lacks the sensitivity necessary for detection of RCS spread on a typical 37- or 25-mm diameter filter. Nonetheless, Zheng et al. [11] demonstrated that concentrating dust samples onto a small area can enhance the sensitivity of portable Raman spectroscopy. Therefore, employing this sample collection technique may facilitate the evaluation of the suitability of functionalized filters for RCS analysis using portable Raman spectroscopy.

It should be noted that colored minerals such as hematite and pyrite present in the coal samples can absorb laser light and contribute to fluorescence issues. The XRD spectrum of the brown coal sample (Figure S1) confirms the presence of pyrite. However, its contribution to fluorescence is relatively minor compared to OC, as evident from the absence of pyrite peaks (341 and 377 cm^{-1}) in the Raman spectra in Figures 3–6. The negligible impact of pyrite is likely due to its low concentration in the coal sample. Assuming all sulfur (2% as shown in Table S1) is in the form of pyrite (FeS_2), the maximum pyrite concentration would be less than 4%.

Several challenges remain for using Raman to quantitatively determine RCS in dust collected on filters. Due to the small area interrogated by the laser beam (<1 to 100 μm in diameter), the microscale inhomogeneity and nonuniformity of particle deposit thickness and composition on the filter causes large variations in Raman signal among different measurement spots on the filters. Heating of the sample by the laser may displace RCS from the analysis spot, and the Raman signal might change with the particle deposit thickness as shown in the TiO_2 peaks in Figure 5. Additionally, optimization is needed to increase the interaction between HAT and the sampled particles.

5 | Conclusion

Raman spectroscopy offers a promising avenue for the rapid detection of RCS directly on filters. However, the presence of interfering OC in coal dust samples poses a significant challenge, as these compounds generate high fluorescence signals and may lead to detector saturation with short integration times when using portable Raman instruments. This study explored a novel approach to functionalize the filters with an anatase TiO_2 based photocatalyst (HAT) to oxidize OC using the Raman laser source, thereby improving RCS analysis. The feasibility was first demonstrated through photocatalytic degradation of OA on HAT_PVC filter, showing that 20 min of visible light irradiation was sufficient to remove 1 mg of OA on HAT_PVC filters.

Photodegradation of the OC in coal samples was further demonstrated by comparing brown coal and brown coal + RCS mixtures on plain and HAT-functionalized filters. The coal D and G band Raman signals reduced over the course several seconds to minutes of consecutive measurements. The reduction of fluorescence reduced interfering background signal and prevented detector saturation, which further allows longer integration time for each analysis. Both effects improve Raman analysis for minerals including RCS. Filtration efficiency and pressure drop tests show that preloading filters with HAT particles does not compromise the filtration performance.

Acknowledgements

This study was primarily supported by the Desert Research Institute Innovation Research Program (IRP) funds supplemented by NIOSH grant 75D30121C11871. The powder X-ray diffractometer was purchased with the support of National Science Foundation (CHE-1429768). We thank Bankole Osho for performing the XRD and some Raman analyses.

Disclosure

The findings and conclusions in this paper are those of the authors and do not necessarily represent the official position of the National

Institute for Occupational Safety and Health (NIOSH), Centers for Disease Control and Prevention (CDC). The mention of any company or product does not constitute endorsement by NIOSH, CDC.

Conflicts of Interest

The authors declare no conflicts of interest.

Data Availability Statement

The data that support the findings of this study are available from the corresponding author upon request.

References

1. S. Misra, A. L. Sussell, S. E. Wilson, and G. S. Poplin, "Occupational Exposure to Respirable Crystalline Silica Among US Metal and Nonmetal Miners, 2000–2019," *American Journal of Industrial Medicine* 66, no. 3 (2023): 199–212.

2. H. Barnes, N. S. L. Goh, T. L. Leong, and R. Hoy, "Silica-Associated Lung Disease: An Old-World Exposure in Modern Industries," *Respirology* 24, no. 12 (2019): 1165–1175.

3. NIOSH, *Quartz in Coal Mine Dust, by IR (Redeposition) - NIOSH Method 7603* (Washington, DC: The National Institute for Occupational Safety and Health (NIOSH), 2003).

4. NIOSH, *Silica, Crystalline, by XRD (Filter Redeposition) - NIOSH Method 7500* (Washington, DC: The National Institute for Occupational Safety and Health (NIOSH), 2003).

5. MSHA, *Infrared Determination of Quartz in Respirable Coal Mine Dust-Method No. MSHA P7* (Pittsburgh, PA: Mine Safety Health Administration, Department of Labor, 2008).

6. MSHA, *X-Ray Diffraction Determination of Quartz and Crystobalite in Respirable Mine Dust -Method No. MSHA P2* (Pittsburgh, PA: Mine Safety Health Administration, Department of Labor, 1989).

7. NASEM, *Monitoring and Sampling Approaches to Assess Underground Coal Mine Dust Exposures* (Washington, DC: National Academies Press, National Academies of Sciences, Engineering, and Medicine, 2018).

8. P. Nascimento, S. J. Taylor, W. P. Arnott, K. C. Kocsis, X. L. Wang, and H. Firouzkouhi, "Development of a Real-Time Respirable Coal Dust and Silica Dust Monitoring Instrument Based on Photoacoustic Spectroscopy," *Mining, Metallurgy & Exploration* 39 (2022): 2237–2245.

9. W. Arnott, C. Kocsis, X. L. Wang, et al., "Real-Time Measurements of Respirable Crystalline Silica, Kaolinite, Coal, and Calcite," in *Underground Ventilation* (London: CRC Press, 2023), 256–263.

10. S. J. Taylor, P. Nascimento, W. P. Arnott, and C. Kocsis, "Real-Time Photoacoustic Measurements of the Mass Concentration of Respirable Crystal Silica Dust: Theory," *Mining, Metallurgy & Exploration* 39, no. 5 (2022): 2247–2256.

11. L. Zheng, P. Kulkarni, M. E. Birch, K. Ashley, and S. Wei, "Analysis of Crystalline Silica Aerosol Using Portable Raman Spectrometry: Feasibility of Near Real-Time Measurement," *Analytical Chemistry* 90, no. 10 (2018): 6229–6239.

12. A. L. Miller, P. L. Drake, N. C. Murphy, J. D. Noll, and J. C. Volkwein, "Evaluating Portable Infrared Spectrometers for Measuring the Silica Content of Coal Dust," *Journal of Environmental Monitoring* 14, no. 1 (2012): 48–55.

13. A. L. Miller, A. T. Weakley, P. R. Griffiths, E. G. Cauda, and S. Bayman, "Direct-on-Filter α-Quartz Estimation in Respirable Coal Mine Dust Using Transmission Fourier Transform Infrared Spectrometry and Partial Least Squares Regression," *Applied Spectroscopy* 71, no. 5 (2017): 1014–1024.

14. J. F. Hart, D. A. Autenrieth, E. Cauda, et al., "A Comparison of Respirable Crystalline Silica Concentration Measurements Using a Direct-on-Filter Fourier Transform Infrared (FT-IR) transmission Method vs. a Traditional Laboratory X-Ray Diffraction Method," *Journal of Occupational and Environmental Hygiene* 15, no. 10 (2018): 743–754.

15. E. L. Ashley, E. Cauda, L. G. Chubb, D. P. Tuchman, and E. N. Rubinstein, "Performance Comparison of Four Portable FTIR Instruments for Direct-on-Filter Measurement of Respirable Crystalline Silica," *Annals of Work Exposures and Health* 64, no. 5 (2020): 536–546.

16. J. D. Pampena, E. G. Cauda, L. G. Chubb, and J. J. Meadows, "Use of the Field-Based Silica Monitoring Technique in a Coal Mine: A Case Study," *Mining, Metallurgy & Exploration* 37, no. 2 (2020): 717–726.

17. R. Stach, T. Barone, E. Cauda, et al., "Direct Infrared Spectroscopy for the Size-Independent Identification and Quantification of Respirable Particles Relative Mass in Mine Dusts," *Analytical and Bioanalytical Chemistry* 412, no. 14 (2020): 3499–3508.

18. E. Cauda, A. Miller, and P. Drake, "Promoting Early Exposure Monitoring for Respirable Crystalline Silica: Taking the Laboratory to the Mine Site," *Journal of Occupational and Environmental Hygiene* 13, no. 3 (2016): D39–D45.

19. B. Osho, M. Elahifard, X. Wang, et al., "Evaluation of PVC and PTFEon Filters for Direct-On-Filter Crystalline Silica Quantification by FTIR," *Journal of Occupational and Environmental Hygiene* (2024). https://doi.org/10.1080/15459624.2024.2357080.

20. P. Stacey, K. T. Mader, and C. Sammon, "Feasibility of the Quantification of Respirable Crystalline Silica by Mass on Aerosol Sampling Filters Using Raman Microscopy," *Journal of Raman Specroscopy* 48, no. 5 (2017): 720–725.

21. P. Stacey, F. Clegg, J. Morton, and C. Sammon, "An Indirect Raman Spectroscopy Method for the Quantitative Measurement of Respirable Crystalline Silica Collected on Filters Inside Respiratory Equipment," *Analytical Methods* 12, no. 21 (2020): 2757–2771.

22. J. Jehlička and P. Vandenabeele, "Evaluation of Portable Raman Instruments With 532 and 785-nm Excitation for Identification of Zeolites and Beryllium Containing Silicates," *Journal of Raman Spectroscopy* 46, no. 10 (2015): 927–932.

23. J. Xu, Q. He, Z. Xiong, et al., "Raman Spectroscopy as a Versatile Tool for Investigating Thermochemical Processing of Coal, Biomass, and Wastes: Recent Advances and Future Perspectives," *Energy & Fuels* 35, no. 4 (2021): 2870–2913.

24. J. Schneider, M. Matsuoka, M. Takeuchi, et al., "Understanding TiO_2 Photocatalysis: Mechanisms and Materials," *Chemical Reviews* 114, no. 19 (2014): 9919–9986.

25. A. Fujishima, T. N. Rao, and D. A. Tryk, "Titanium Dioxide Photocatalysis," *Journal of Photochemistry and Photobiology, C: Photochemistry Reviews* 1, no. 1 (2000): 1–21.

26. M. R. Elahifard, S. Rahimnejad, S. Haghighi, and M. R. Gholami, "Apatite-Coated Ag/AgBr/TiO_2 Visible-Light Photocatalyst for Destruction of Bacteria," *Journal of the American Chemical Society* 129, no. 31 (2007): 9552–9553.

27. M. Azimzadehirani, M. Elahifard, S. Haghighi, and M. Gholami, "Highly Efficient Hydroxyapatite/TiO_2 Composites Covered by Silver Halides as *E. coli* Disinfectant Under Visible Light and Dark Media," *Photochemical & Photobiological Sciences* 12, no. 10 (2013): 1787–1794.

28. C. Hu, Y. Lan, J. Qu, X. Hu, and A. Wang, "Ag/AgBr/TiO_2 Visible Light Photocatalyst for Destruction of Azodyes and Bacteria," *Journal of Physical Chemistry B* 110, no. 9 (2006): 4066–4072.

29. M. R. Elahifard and M. R. Gholami, "Acid Blue 92 Photocatalytic Degradation in the Presence of Scavengers by Two Types Photocatalyst," *Environmental Progress & Sustainable Energy* 31, no. 3 (2012): 371–378.

30. M. R. Elahifard, S. Rahimnejad, R. Pourbaba, S. Haghighi, and M. R. Gholami, "Photocatalytic Mechanism of Action of Apatite-Coated Ag/AgBr/TiO_2 on Phenol and *Escherichia coli* and *Bacillus subtilis* Bacteria Under Various Conditions," *Progress in Reaction Kinetics and Mechanism* 36, no. 1 (2011): 38–52.

31. S. Ahmadvand, M. Elahifard, M. Jabbarzadeh, et al., "Bacteriostatic Effects of Apatite-Covered Ag/AgBr/TiO2 Nanocomposite in the Dark: Anomaly in Bacterial Motility," *Journal of Physical Chemistry B* 123, no. 4 (2019): 787–791.

32. C. Analytical Methods, "Evaluation of Analytical Instrumentation. Part XIX CHNS Elemental Analysers," *Accreditation and Quality Assurance: Journal for Quality, Comparability and Reliability in Chemical Measurement* 11, no. 11 (2006): 569–576.

33. J. C. Hower, R. B. Finkelman, C. F. Eble, and B. J. Arnold, "Understanding Coal Quality and the Critical Importance of Comprehensive Coal Analyses," *International Journal of Coal Geology* 263 (2022): 104120.

34. P. Stacey, E. Kauffer, J.-C. Moulut, et al., "An International Comparison of the Crystallinity of Calibration Materials for the Analysis of Respirable α-Quartz Using X-Ray Diffraction and a Comparison With Results From the Infrared KBr Disc Method," *Annals of Occupational Hygiene* 53, no. 6 (2009): 639–649.

35. A. L. Miller, N. C. Murphy, S. J. Bayman, et al., "Evaluation of Diffuse Reflection Infrared Spectrometry for End-of-Shift Measurement of α-Quartz in Coal Dust Samples," *Journal of Occupational and Environmental Hygiene* 12, no. 7 (2015): 421–430.

36. T. Luttrell, S. Halpegamage, J. Tao, A. Kramer, E. Sutter, and M. Batzill, "Why Is Anatase a Better Photocatalyst Than Rutile?—Model Studies on Epitaxial TiO_2 Films," *Scientific Reports* 4, no. 4043 (2014): 1–8.

37. J. C. Chow, J. G. Watson, X. Wang, B. Abbasi, W. R. Reed, and D. Parks, "Review of Filters for Air Sampling and Chemical Analysis in Mining Workplaces," *Minerals* 12, no. 10 (2022): 1314.

38. J.-C. Soo, K. Monaghan, T. Lee, M. Kashon, and M. Harper, "Air Sampling Filtration Media: Collection Efficiency for Respirable Size-Selective Sampling," *Aerosol Science and Technology* 50, no. 1 (2016): 76–87.

39. M. M. Kosanić, "Photocatalytic Degradation of Oxalic Acid Over TiO_2 Power," *Journal of Photochemistry and Photobiology A: Chemistry* 119, no. 2 (1998): 119–122.

40. S. Potgieter-Vermaak, N. Maledi, N. Wagner, J. Van Heerden, R. Van Grieken, and J. Potgieter, "Raman Spectroscopy for the Analysis of Coal: A Review," *Journal of Raman Spectroscopy* 42, no. 2 (2011): 123–129.

41. M. Elahifard, R. Behjatmanesh-Ardakani, S. Ahmadvand, B. Abbasi, and B. Abbasi, "A Mechanistic Study of Photo-Oxidation of Phenol and AB92 by AgBr/TiO_2," *Research on Chemical Intermediates* 45 (2019): 4885–4896.

Supporting Information

Additional supporting information can be found online in the Supporting Information section.